ELSEVIER

Journal of African Earth Sciences 35 (2002) 51–60

Journal of African Earth Sciences

www.elsevier.com/locate/jafrearsci

Geochemistry of the quartz diorite—granite association, Roded area, southern Israel

Ron Bogoch [a,*], Dov Avigad [b], Tuvia Weissbrod [a]

[a] Geological Survey of Israel, 30 Malkhe Israel Street, Jerusalem 95501, Israel
[b] Department of Geology, The Hebrew University of Jerusalem, Jerusalem 91904, Israel

Accepted 20 May 2002

Abstract

The Roded quartz diorite of southern Israel formed by fractional crystallization of source magma probably derived from melting in a subduction zone slab. There is little evidence of either magma mixing or large-scale crustal contamination. Metamorphic xenoliths derive from either nearby country-rock or from sources at depth. Enclaves with igneous textures are mafic micro-granular enclaves with the geochemical characteristics of calc-alkaline I-type plutons.

The granite, wholly contained within the quartz diorite, formed in irregularly spaced "pockets" near the end of quartz diorite crystallization from a late-stage residual liquid. The granite retains certain of the I-type characteristics of the quartz diorite. The aplitic nature of the granite bodies suggests initially high nucleation rates coupled with rapid cooling, the micro-shear veinlets having formed from high pressures in a late, volatile- and H_2O-rich phase.

Keywords: Quartz diorite; Granite; Geochemistry; Slab-melt; Neoproterozoic; Israel

1. Introduction

Diorites are among the most intriguing plutonic rocks for petrogenetic studies (Bonin and Giret, 1990). This relates in part to their occurrence in varying geological environments and to the presence of various salient, sometimes enigmatic features such as schlieren and various enclaves. Expect for clearly defined wall-rock xenoliths, the origin of the enclaves and their interaction with their host rocks is largely controversial.

The Neoproterozoic Roded quartz diorite of southern Israel exhibits heterogeneity in mineralogical and chemical composition, and contains enclaves of varying size, shape and chemistry. The quartz diorite is further complicated by the presence of numerous small leucocratic granite bodies apparently confined wholly within its boundaries. Using data from field mapping, petrography, and mineral and whole rock chemistry, we have attempted to determine the origin of these features together with their host rock.

2. Geological setting

The Precambrian outcrops of southern Israel (totaling ~90 km^2) occur within the northern surficial extension of the Neoproterozoic Arabian–Nubian Shield (ANS, Fig. 1). The orogenic cycle of the ANS first involved different stages of accretion resulting from the juxtaposition of juvenile island arc belts along ophiolite-bearing suture zones (Kröner, 1993; Stern, 1993; Stoesser and Camp, 1985). This was followed by large-scale calc-alkaline plutonism, cratonization and ultimately continental collision leading to accretion with the pre-Neoproterozoic African plate. Many granitoids in the ANS were classified by Bentor (1985) as alkaline to peralkaline, which together with non-metamorphosed volcanic and continental clastic sedimentary rocks represent a Neoproterozoic extensional phase. The age of the Roded quartz diorite is determined at approximately 630 Ma (U–Pb zircon, Katz et al., 1998; Stein and Goldstein, 1996).

3. Field description

The Roded quartz diorite covers an area of 7 × 2 km and is part of a tectonically isolated Precambrian block

* Corresponding author.
E-mail address: ron.bogoch@mail.gsi.gov.il (R. Bogoch).

0899-5362/02/$ - see front matter
PII: S0899-5362(02)00038-6

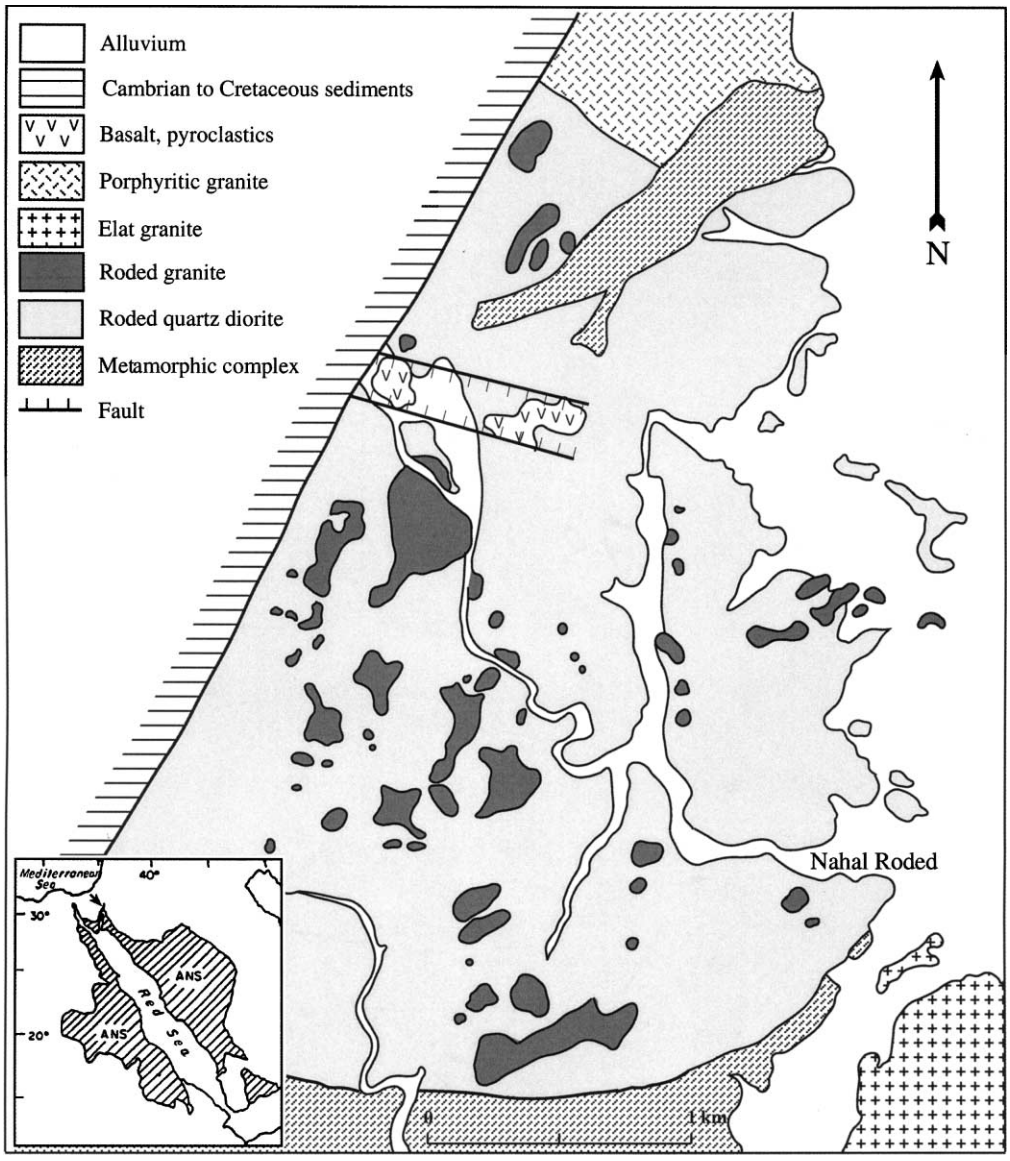

Fig. 1. Schematic geological map of the Roded area, southern Israel (modified after Weissbrod (1961)). Insert: arrow shows location of study area; ANS—Arabo-Nubian Shield.

in southern Israel (Fig. 1). It is overlain to the east by alluvium and Neogene sedimentary rocks, to the west with down-faulted Cambrian to lower Cretaceous sandstone, and intrudes upper greenschist to amphibolite facies metasedimentary and metavolcanic rocks.

The area lies within an arid rocky desert. Exposures are excellent, with weathering resulting in slightly crumbly exposures of generally fresh rock. The topography is rugged, with maximum vertical variations of some 200 m. The quartz diorite is grey on both fresh and weathered surfaces. It is generally medium- to coarse-grained and has a monotonous field appearance.

Scarce but widespread enclaves are present within the quartz diorite, making up $<0.1\%$ of the exposures. These include clearly identifiable country rock xenoliths less than $\sim$30 cm in diameter with roughly elliptical shapes. Certain enclaves are foliated and biotite-amphibole-rich, apparently unlike nearby metamorphic rocks and possibly derived from a greater depth. The majority of the enclaves are light to dark grey, fine-grained and range in size from a few cm to $\sim$30 cm.

Hard, dense, generally fine-grained leucocratic granite covers some 5% of the quartz diorite pluton, and forms the peaks of higher hills. The granite is clearly intrusive with sharp contacts and, in places, sill-like bodies extend from the granite into the quartz diorite. Chill zones are not observed and xenoliths are absent. The granite bodies vary in size from a few to several hundred meters in diameter, and their distribution on the map suggest a 'splattering' of finger paint. Individual bodies vary in shape from "irregular ellipses" to "amoebic". When observed in vertical section, all bodies

are close to horizontal. Most exposures exhibit a myriad of fine, linear brownish veinlets, seen in thin section as healed micro-fractures or micro-shears. These show no preferred orientation, are locally criss-crossed, or radiate fishbone-like, from a "central", slightly thicker veinlet. Pegmatites were not found in association with these granites.

The Precambrian country rocks intruded by the quartz diorite to its south consist of plagioclase–quartz–biotite–garnet schists and plagioclase–quartz–biotite–amphibole gneisses, banded gneisses and migmatites, and to the north of plagioclase–biotite–amphibole schists and coarse-grained porphyritic granite. The dominant trend of lineation and foliation is ~N–S. A coarse grained biotite-granite (mapped as Elat granite) occurs to the southeast in the metamorphic complex. Although not in contact with the quartz-diorite, its pegmatites do occur within the latter. Both magnetic and gravity maps of southernmost Israel indicate that the Roded quartz diorite body is significantly larger in the subsurface (Segev et al., 1999), suggesting that the present exposures represent a relatively high level of the intrusion. Al-hornblende barometry and amphibole–plagioclase thermometry suggest crystallization of the quartz diorite at 2–3 kbar and ~700 °C (Katz et al., 1998). The quartz-diorite and associated country rock are crossed by numerous fine-grained porphyritic basaltic andesite to rhyolitic dykes.

4. Petrography

The main plutonic body consists of quartz diorite and subsidiary tonalite to quartz monzodiorite. The rocks are hypidiomorphic to xenomorphic inequigranular (major minerals: 0.5–3 mm). Although it has a rather monotonous appearance in the field, the quartz diorite shows variations in the proportions of plagioclase (50–60%), quartz (15–20%), biotite (5–10%), hornblende (4–10%), and K-feldspar (1–3%). Plagioclase (oligoclase–andesine) forms a touching framework of crystals, the interstices filled by quartz (±K-feldspar). Twin planes in plagioclase extend to the edges of the grains, although there is generally a very slight increase of sodium and depletion of calcium at the rims. Similar zoning was noted in hornblende. There is no correlation between the amounts of biotite and hornblende, although biotite usually dominates. The K-feldspar content increases with increasing biotite. The melanocratic minerals occur together and their texture suggests sequential crystallization—(rare) clinopyroxene in cores of ferroan edenitic hornblende crystals, which are commonly rimmed by biotite (Byron et al., 1994). In places clinopyroxene is outlined by fine blebs of magnetite. The relative lack of pyroxene may thus be due to reactions (and resorption) to hornblende and biotite with increasing H_2O and decreasing temperature during differentiation. Accessory minerals are titanite (up to several %), zircon, magnetite, and apatite. Minor alteration products are sericite, chlorite and calcite.

The "diorite-like" fragments within the quartz diorite are possible candidates for mafic micro-granular enclaves (MMEs), which are defined by Didier and Barbarin (1991) as blobs of coeval magma, mostly with sharp contacts, ovoid shapes and fine-grained textures, which were introduced during mixing and which crystallized simultaneously with their host. The mineralogy of the MMEs is similar to the quartz diorite but their modes vary considerably with 45–64% plagioclase, 1–14% quartz, 7–27% biotite and 9–30% hornblende. Their textures are magmatic (fine-grained), but the rocks show a great deal of petrographic diversity; e.g., plagioclase and/or amphibole phenocrysts; some are equigranular or not; presence or not of aligned plagioclase laths; presence or not of ophitic texture. It is thus difficult to define a single enclave type with consistent mineralogy and texture.

The granites are very fine-grained with a xenomorphic granular texture, dominated by albite (40–50%), K-feldspar (10–25%) and quartz (30–35%), generally with traces of biotite, muscovite, titanite, zircon and spots of iron oxide. Biotite content increases slightly in coarser (~2 mm) varieties. The micro-shears vary in width from <1 to 3–4 mm, and consist of tiny angular fragments of feldspar and quartz healed by quartz and amorphous silica. The composition of the feldspar fragments in the fractures appears to be identical with that in the granite host.

5. Geochemistry

5.1. Methods

Major and trace elements were measured in the Geochemical Laboratory, Geological Survey of Israel by inductively coupled plasma-atomic emission spectroscopy (ICP-AES) and inductively coupled plasma-mass spectrometry (ICP-MS). For major elements, samples were heated to 1050 °C, fused with $LiBO_2$ and dissolved in HNO_3. For trace elements, samples were sintered with Na_2O_2 and dissolved in HNO_3. Accuracy for major elements is 2% and for trace elements, 10%.

Mineral analyses were made using JEOL 840 SEM with attached Link 10,000 energy-dispersion spectrometer (EDS: ZAF4 program) on polished sections (comparison with standard block files).

5.2. Mineral chemistry

Representative mineral analyses are presented in Table 1. The chemistry of the main minerals in the

Table 1
Representative analyses (wt.%) of (A) feldspar, (B) amphibole and pyroxene, (C) biotite. Minerals were normalized as follows: Fsp to 8O; Amph to 23O, cations Si + Ti + Al + total Fe + Mn + Mg = 13; Pyx to 6O; Bt to 22O

(A)	Quartz diorite				Granite		Enclaves		
	RD-43 (core)	RD-43 (rim)	RD-39	D-212	R-35	R-36	D-204a	R-21	RD-29
SiO_2	63.18	64.34	62.39	60.94	66.81	63.57	60.67	64.56	62.09
Al_2O_3	22.49	23.3	22.95	23.9	19.98	17.21	24.26	22.17	23.18
CaO	5.57	4.9	6.07	6.99	1.31	–	7.27	4.0	6.47
Na_2O	7.5	7.85	7.01	7.16	9.34	0.41	6.85	8.59	6.62
K_2O	0.26	0.26	0.71	0.28	0.89	18.4	0.19	0.14	0.71
Total	99.0	100.65	99.13	99.27	98.33	99.59	99.24	99.46	99.07
Si	2.815	2.814	2.787	2.728	2.970	2.997	2.715	2.853	2.776
Al	1.181	1.201	1.208	1.261	1.047	0.956	1.279	1.155	1.221
Ca	0.266	0.230	0.290	0.335	0.062	–	0.349	0.189	0.310
Na	0.648	0.666	0.607	0.621	0.805	0.037	0.594	0.736	0.574
K	0.015	0.015	0.040	0.016	0.050	1.107	0.011	0.008	0.040
An	28.6	25.3	31.0	34.5	6.8	–	36.6	20.3	33.6
Ab	69.8	73.1	64.8	63.9	87.8	3.2	62.3	78.9	62.1
Or	1.6	1.6	4.2	1.6	5.4	96.8	1.1	0.8	4.3

(B)	Quartz diorite						Enclaves				
	D-212	RD-43	RD-39 (core)	RD-39 (rim)	RD-39	RD-39 (Pyrox.)	D-79b	D-204a	D-207 (Pheno.)	RD-26 (core)	RD-26 (rim)
SiO_2	42.66	45.12	41.67	42.13	45.58	50.15	47.24	43.52	45.0	47.56	48.3
TiO_2	1.96	1.19	2.0	2.19	1.29	0.25	0.99	1.3	1.02	0.76	0.78
Al_2O_3	7.76	5.23	6.97	7.43	5.25	0.76	6.09	7.83	7.61	5.52	5.29
FeO^t	19.09	18.51	21.21	21.5	20.07	11.24	16.36	19.39	18.92	16.12	16.74
MnO	0.28	0.34	0.48	0.34	0.43	0.66	–	0.51	0.43	0.59	0.01
MgO	11.1	11.6	9.43	9.66	10.56	11.08	12.9	10.35	10.9	13.17	12.89
CaO	13.84	13.47	12.93	13.2	13.93	25.48	13.51	13.32	13.56	13.59	13.85
Na_2O	1.42	0.88	1.42	1.43	0.97	0.59	1.34	1.27	1.03	1.23	1.01
K_2O	0.77	0.67	1.07	0.97	0.74	–	0.78	0.53	0.47	0.33	0.39
Total	98.88	97.01	97.18	98.85	98.82	100.21	99.21	98.02	98.94	98.87	99.26
Si	6.447	6.881	6.483	6.429	6.922	1.889	6.975	6.587	6.713	7.010	7.109
Ti	0.223	0.136	0.234	0.251	0.147	0.007	0.110	0.148	0.114	0.084	0.086
Al	1.382	0.940	1.278	1.336	0.939	0.033	1.060	1.397	1.338	0.959	0.918
Fe	2.413	2.361	2.759	2.744	2.548	0.355	2.020	2.464	2.361	1.987	2.061
Mn	0.035	0.043	0.063	0.043	0.055	0.021	–	0.065	0.054	0.074	0.001
Mg	2.500	2.638	2.188	2.197	2.390	0.623	2.839	2.335	2.424	2.893	2.829
Ca	2.241	2.201	2.156	2.158	2.266	1.029	2.137	2.160	2.167	1.148	1.183
Na	0.416	0.260	0.428	0.423	0.285	0.043	0.383	0.373	0.298	0.351	0.288
K	0.148	0.130	0.213	0.188	0.143	–	0.147	0.102	0.090	0.062	0.073

(C)	Quartz diorite				Granite		Enclaves				
	RD-43	RD-29	D-212	RD-18	D-39	D-39	D-79b	RD-26	RD-26	RD-19	D-124
SiO_2	35.24	36.02	35.67	35.85	36.9	39.27	36.72	36.29	36.16	36.3	37.04
TiO_2	4.47	4.38	4.52	4.23	2.29	2.21	3.52	2.99	3.09	3.35	2.06
Al_2O_3	13.95	13.48	13.38	13.81	13.74	13.39	13.27	13.95	13.79	13.53	14.48
FeO^t	22.67	21.24	21.97	23.86	23.84	21.71	21.19	21.11	21.16	21.35	22.48
MnO	0.35	0.26	–	0.44	0.41	0.47	0.29	–	0.29	–	0.26
MgO	10.71	11.94	11.91	9.33	11.96	12.84	12.24	12.53	12.39	12.67	15.32
K_2O	11.26	10.97	10.5	11.15	9.58	8.01	11.52	11.25	11.06	10.95	7.28
Total	98.65	98.29	97.95	98.67	98.72	97.9	98.75	98.12	97.94	98.15	98.92
Si	5.374	5.456	5.426	5.484	5.569	5.824	5.542	5.487	5.493	5.488	5.448
Al	2.507	2.407	2.399	2.490	2.444	2.340	2.361	2.486	2.470	2.411	2.510
Ti	0.513	0.499	0.517	0.487	0.26	0.246	0.400	0.340	0.353	0.381	0.228
Mg	2.435	2.696	2.701	2.128	2.691	2.839	2.754	2.825	2.806	2.856	2.359
Mn	0.045	0.033	–	0.057	0.052	0.059	0.037		0.037	–	0.032
Fe	2.891	2.691	2.795	3.052	3.009	2.693	2.891	2.965	2.644	2.691	2.693
K	2.190	2.120	2.038	2.176	1.845	1.515	2.218	2.170	2.143	2.112	1.366

Table 2
Representative analyses of quartz diorite, granite and magmatic enclaves (major element oxides in wt.%, trace elements in ppm)

	Quartz diorite					Granite					Enclaves				
	D-77	D-93	R-39	D-200	R-43	R-10	R-15	R-34	R-35	R-282	D-79	D123b	R-21	R-26	R-41
SiO_2	63.2	65.0	62.5	58.3	61.0	79.0	75.5	75.0	78.8	77.5	57.6	61.7	64.5	53.8	60.0
TiO_2	0.8	0.6	0.7	0.9	0.9	0.1	<0.1	0.1	<0.1	0.06	1.4	0.7	0.8	1.1	0.8
Al_2O_3	15.5	15.3	16.3	16.7	16.1	12.1	13.9	14.7	12.1	11.4	6.2	15.6	16.1	16.4	14.5
Fe_2O_3	6.0	3.9	4.0	6.2	5.9	0.9	1.1	1.3	0.9	1.1	10.7	5.4	4.6	8.0	6.2
MnO	0.08	0.05	0.07	0.08	0.07	<0.05	<0.05	<0.05	<0.05	<0.05	0.15	0.07	0.06	0.1	0.1
MgO	3.5	2.8	3.5	4.9	4.3	0.2	<0.1	0.3	<0.1	<0.1	11.4	4.6	2.7	7.2	6.8
CaO	4.4	3.4	4.6	5.6	4.6	0.2	0.7	0.5	0.2	0.3	7.4	4.7	3.6	6.8	6.0
Na_2O	4.3	5.0	4.1	4.7	4.2	2.8	4.2	4.5	3.6	3.7	0.8	4.2	3.3	4.1	3.2
K_2O	1.7	2.5	1.9	1.3	1.8	4.5	4.0	3.3	4.1	4.8	1.8	2.0	3.6	1.6	1.4
P_2O_5	0.1	0.1	0.2	0.2	0.2	<0.1	<0.1	<0.1	<0.1	<0.1	0.2	0.1	0.2	0.4	0.3
Loi	0.9	1.4	1.5	1.5	0.7	0.4	0.6	0.5	0.2	1.1	2.5	1.5	1.2	1.3	1.4
Total	100.48	100.05	99.37	100.38	99.88	100.2	100.1	100.2	100.0	100.0	99.15	100.57	100.66	100.8	100.7
Rb	32	33	39	27	51	82	102	91	98	90	48	40	61	31	35
Sr	964	660	908	1016	996	34	69	361	6	20	42	821	925	1080	912
Ba	797	674	859	560	558	170	266	663	68	75	513	884	975	713	974
Zr					200	140	60	100	155				190	190	175
Sc		7.6	8.8	13	11	0.5	2.1	2.2	0.4				8.6	16	19
Co		12	14	24	21	1.6	1.0	2.2	0.8	5			13	34	32
Ni	92	78	101	124	129	24	24	25	22	22	326	133	62	203	190
Nb	16	10	8	13	9					2.3	17	15	4	13	14
Pb	20	16	33	24	44	32	42	36	21	11	8	24	26	28	34
Zn	62	58	73	73	84	30	17	38	26	20	129	71	65	110	75
Y	8	8	13	10	11	5	12	8	33	46.5	21	10	8.4	13.6	10.5
La	20.8	19.1	22.6	18.5	12.8	6.5	7.4	7.1	16.2	21.5	21.0	17.4	26.4	17.5	17.6
Ce	43.3	39.5	52.4	41.7	28.6	16.1	15.4	15.8	39.4	67.0	57.1	40.0	54.2	43.0	39.2
Pr	5.35	5.18	6.45	5.68	3.75	1.17	1.90	1.91	5.50	6.9	8.66	5.33	6.58	6.31	5.0
Nd	20.9	21.1	25.1	23.9	15.3	4.07	7.05	7.08	23.6	29.5	40.1	22.1	25.3	28.2	20.8
Sm	3.59	3.82	4.41	4.49	2.86	0.62	1.64	1.66	6.5	8.4	8.6	4.08	4.35	5.57	3.78
Eu	1.10	0.94	1.04	1.23	0.72	0.09	0.06	0.43	0.10	0.26	1.14	1.06	1.21	1.40	1.08
Gd	3.0	3.2	3.95	3.01	2.52	0.58	1.65	1.66	7.76	9.1	7.64	3.58	3.52	4.73	3.4
Tb	0.38	0.41	0.53	0.49	0.32	0.08	0.27	0.28	1.26	1.47	1.04	0.47	0.45	0.60	0.45
Dy	1.73	1.87	2.48	2.23	1.56	0.36	1.54	1.55	7.32	7.1	5.11	2.11	1.94	2.73	2.13
Ho	0.32	0.35	0.50	0.42	0.29	0.07	0.29	0.39	1.49	1.4	0.94	0.40	0.37	0.51	0.4
Er	0.96	1.00	1.56	1.21	0.83	0.24	0.84	0.92	4.15	4.3	2.61	1.18	1.07	1.47	1.2
Tm	0.13	0.13	0.21	0.15	0.11	0.03	0.12	0.14	0.56	0.52	0.34	0.16	0.13	0.18	1.14
Yb	0.85	0.85	1.30	0.95	0.71	0.48	0.77	0.92	3.20	3.1	2.05	1.0	0.87	1.16	0.96
Lu	0.13	0.13	0.19	0.13	0.10	0.05	0.10	0.13	0.46	0.45	0.31	0.15	0.12	0.17	0.15
Cs		0.7	1.7	1.3	1.8	0.5	2.0	3.1	0.3				1.6	1.4	1.4
Hf		4.9	4.3	3.2	4.6	3.9	2.6	2.2	5.2				3.8	4.2	4.3
Ta		<0.5	<0.5	<0.5	<0.5	<0.5	<0.5	0.5	0.2	0.13			<0.5	0.2	0.4
U		0.4	1.6	0.7	1.7	0.6	2.0	1.3	1.6	1.5			1.3	0.2	0.8
Th		1.6	3.9	2.7	3.2	5.3	5.1	4.7	4.7	6.9			4.7	0.5	2.2
Sr/Y	120.5	82.5	69.8	101.6	90.5	6.8	5.8	0.2	0.2	0.4	2	82.1	110	79.4	86.9
La/Yb	24.5	22.5	17.4	19.5	18	13.5	9.6	5.1	7.7	6.9	10.2	17.4	30.3	15.1	18.3

quartz diorite is fairly homogeneous, whereas there are greater variations of mineral compositions within the enclaves. The more mafic the enclaves, the somewhat higher the MgO content in the amphiboles and biotites, although in the quartz diorite these minerals are significantly richer in TiO_2, and for the amphibole, in total iron and K_2O. Biotites from quartz diorite and enclaves plot in the calc-alkaline field in the discrimination diagrams of Abdel-Rahman (1994).

5.3. Whole rock chemistry

Major and trace element compositions of representative lithologies are presented in Table 2 and in Figs. 2 and 3. Only enclaves with apparent igneous textures are shown.

The quartz diorites vary in silica contents between ~58 and 65%, and are metaluminous. Excepting Na_2O, the major element oxides vs. SiO_2 diagrams display linear trends (Figs. 2 and 3). SiO_2 vs K_2O (Peccerillo and Taylor, 1976) and SiO_2 vs $Na_2O + K_2O$ (Barker and Arth, 1976) diagrams suggest that the bulk of the samples plot in the calc-alkaline field. The trace element data

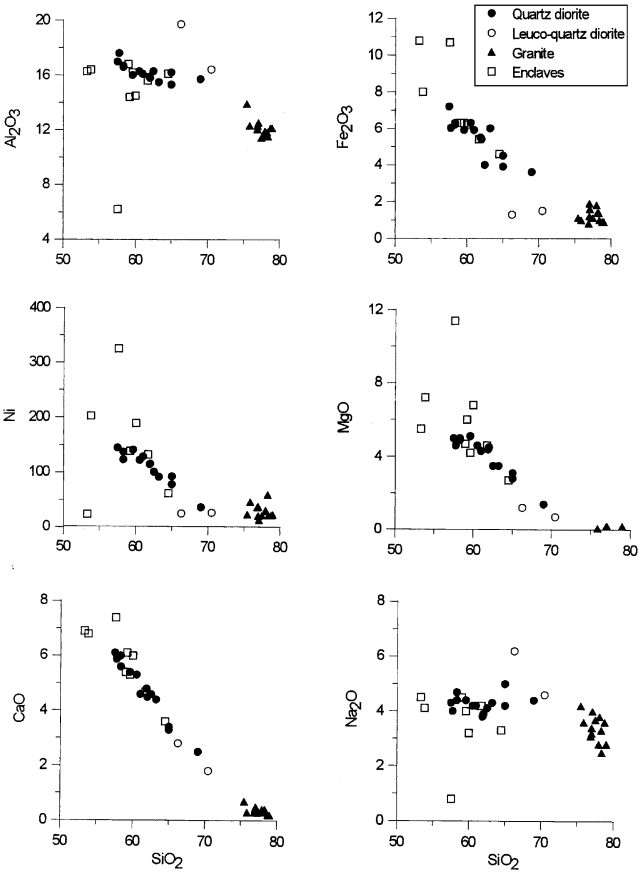

Fig. 2. Variation diagrams of major and trace elements vs silica. Note clustering of granite data generally along trends of the quartz diorite, and in most cases, scatter of enclave data.

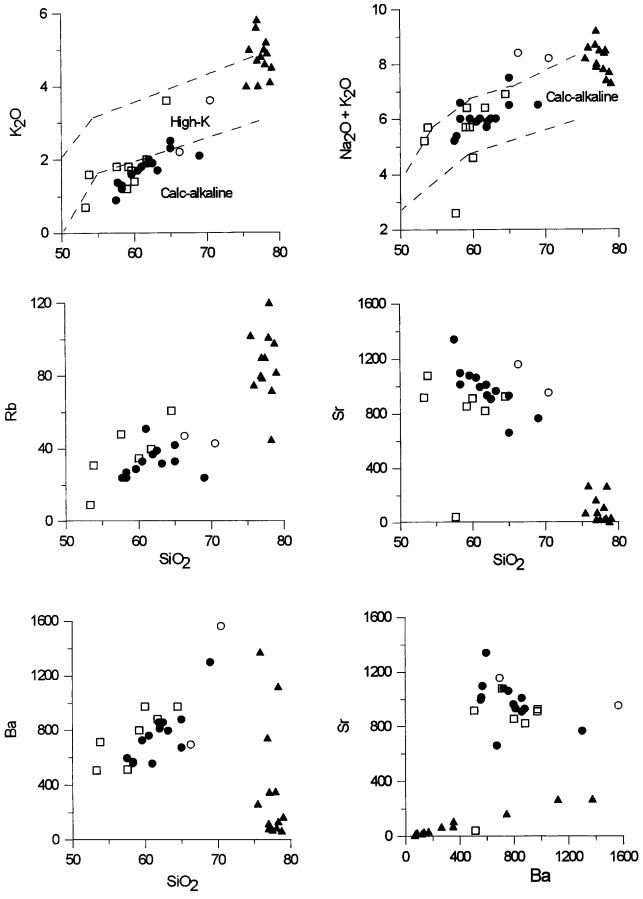

Fig. 3. Variation diagrams of major and trace elements vs silica. Fields in K_2O vs SiO_2 after Peccerillo and Taylor (1976) and the $Na_2O + K_2O$ vs SiO_2 after Barker and Arth (1976). Note scatter of granite data parallel to the y-axis in the Rb and Ba vs SiO_2 diagrams. The only linear correlation found in the granites is Sr vs Ba. Legend as in Fig. 2.

are also commensurate with fractional crystallization, with lower Sr, REE, Sc and the transition metals (e.g., Ni), and with higher Rb and Ba relative to an increase of the SiO_2. These rocks plot in the volcanic arc granite field in both the Rb vs Y + Nb (Fig. 4) and Nb vs Y discrimination diagrams of Pearce et al. (1984). The quartz diorites behave homogeneously on the chondrite-normalized REE plots, with La_N:$Yb_N \sim 13$, fairly flat HREE from Dy to Lu, and negative Eu anomalies (Fig. 5). The ASI (Aluminium Saturation Index, molar Al_2O_3/Na_2O+K_2O+CaO) for all but two samples is <1, and molar Al_2O_3/Na_2O+K_2O is higher than one, indicating that these are metaluminous I-type granitoids. They are characterized by depletion in Rb, Th, Nb and Ti and enrichment in Ba, K, Sr and Zr relative to the primodial mantle (Chappell, 1999; Sun and McDonough, 1989) (Fig. 6). These spikes are identical with those obtained for adakites (Rapp et al., 1999).

The granites are rich in silica, from 75.5% to 79% SiO_2. In Harker diagrams, the major and trace element

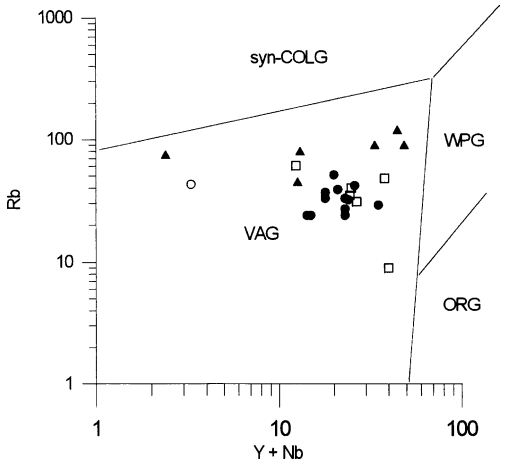

Fig. 4. Rb vs Yb + Nb discrimination diagram (Pearce et al., 1984). Legend as in Fig. 2.

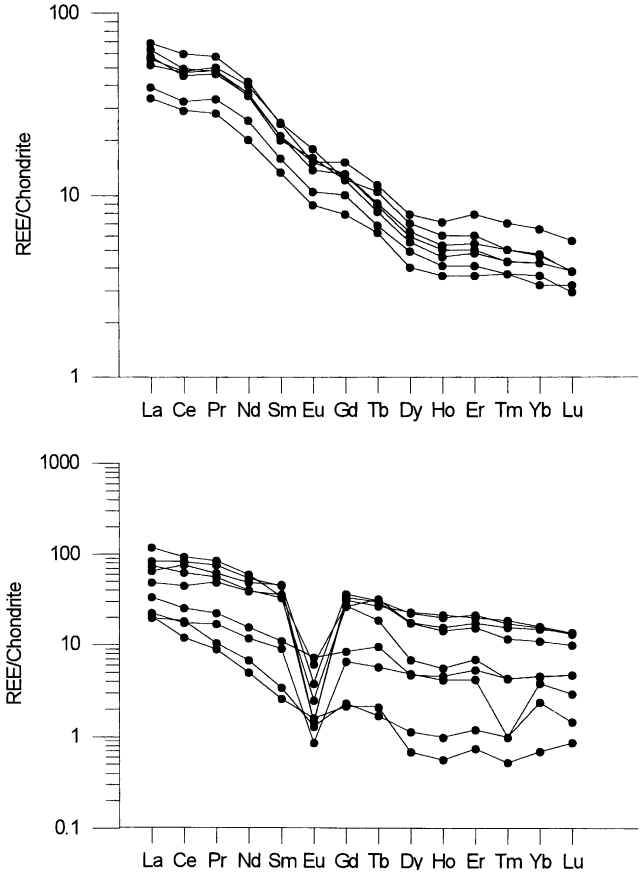

Fig. 5. REE normalized to chondrite. Top: Quartz diorite; bottom: Granite.

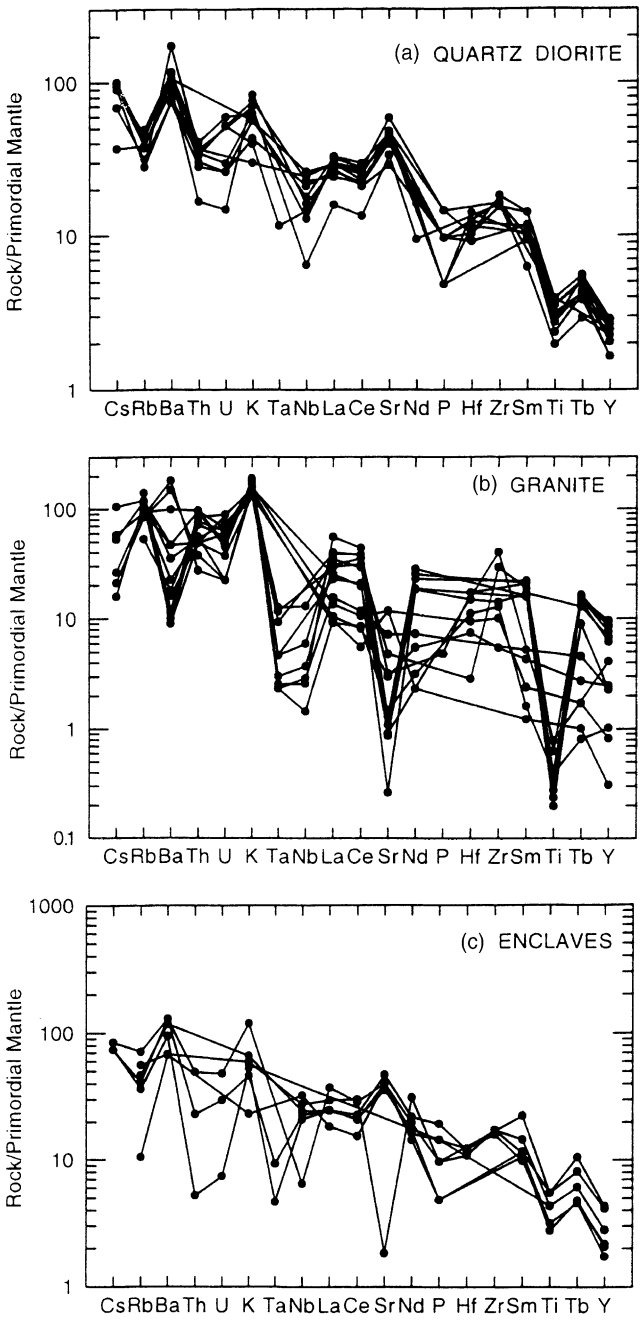

Fig. 6. Multi-element ("spider") diagram of quartz diorite (a), granite (b) and enclaves (c) normalized to primoidial mantle of Wood et al. (1979). Note depletion of Sr in the granite data, and spread of enclave data.

compositions of the granites tend to cluster (partly as a function of the small range of silica values), or spread more or less vertically parallel to the *y*-axis of the diagrams (Rb, Ba, REE, Hf; e.g., Fig. 3). Sr and Ba show a good correlation in the granites whereas an opposite trend occurs in the quartz diorites. In most of the variation diagrams, the granite lies along or close to the trends defined by quartz diorite rocks (Figs. 2 and 3). The REE show a large distribution of compositions (Fig. 5). A negative anomaly occurs in all samples, varying nearly 10-fold from Eu/Eu^* ~0.05 to ~0.5 (weaker anomalies in samples with lower total REE values). The average ASI of granites is 1.08, and with only two exceptions, overlaps with the ASI values in the quartz diorite.

In a set of igneous enclaves plotted in Harker-type diagrams (Figs. 2 and 3), four samples consistently plot along the trends of the main intrusive suite.

6. Discussion

The Roded quartz diorite is I-type, but differs from fractionated and unfractionated I-type granitoids (Chappell, 1999) in its distinctly higher Sr and lower Y values. These differences suggest that the quartz diorite, unlike the Australian I-type granitoids, was not partly derived from the continental crust (Drummond et al., 1994). It exhibits many of the geochemical features of magmas derived from the melting of a subducting slab (MORB converted into amphibolite or eclogite). Such melts are characterized by Yb $<$ 1.9 ppm, Y $<$ 15 ppm, Sr $>$ 600 ppm, Sr/Y $>$ 40, La/Yb $\geqslant$ 20, and Nb $\leqslant$ 10–11 at 70% SiO_2 and 15% Al_2O_3 (Drummond et al., 1994) all of which correspond to the features of Roded quartz diorite. The slab-melt geochemical signature is further shown by strong geochemical similarity between the Roded quartz diorite and adakites. However, the high $Mg/Mg + Fe^{total}$ ratios ($\sim$0.7–0.8), suggests that they formed by the "hybridization of slab melts with peridotite" (Rapp et al., 1999).

Fractionation of plagioclase and pyroxene can explain the linear trends of major oxides and trace elements in the Harker-type diagrams. On the other hand, residual effects of partial melting are noted, such as depletion in incompatible elements. Relative to adjacent elements in geochemical arrays of primitive mantle normalised multi-element diagrams, Sr, Ba and K are consistently enriched, while Rb, Nb, P and Ti are depleted (Fig. 6). The enrichment in LILE and depletion in HFSE are typical of arc magmatism (e.g., Parada et al., 1999; Shaw et al., 1993).

An active continental margin setting conforms to the calc-alkaline character of the quartz diorite and its timing in the waning compressional stages of the northern part of the Neoproterozoic Arabo-Nubian Shield (ANS). The (meta-) sedimentary rocks (pelites and sandstones), which are the dominant host lithology, are compatible with this setting. In this environment, four components may be involved in magma generation: the subducted slab of oceanic lithosphere, the overlying asthenospheric mantle wedge, the subcontinental mantle, and the continental crust (Wilson, 1989). The data in this paper indicate that the melting of a subducting slab was the main process during the genesis of the quartz diorite.

The physical characteristics of the granites may be summarized as follows: (1) they appear to be solely hosted by the quartz diorite; (2) their total volume relative to the quartz diorite is small; (3) certain of the bodies have sill-like extensions into the quartz diorite; (4) chill-zones were not observed; (5) they do not have associated pegmatites; (6) their configuration in plan is elliptical-"amoebic", and in section, horizontal to subhorizontal ("rootless"); (7) there are no xenoliths of any type present; (8) they are fine grained; phenocrysts are absent; variations in grain size within single granite occurrences were not noted; (9) metasomatic alteration of the quartz diorite near the contacts was not observed; (10) they are crossed by veinlets of healed micro-shears, which do not continue into the quartz diorite.

Based on these features, a genetic relationship between the granite and quartz diorite can be supported. The proposed scenario is that the granite was formed in irregularly spaced "pockets" near the end of quartz diorite crystallization from a late stage residual liquid.

The aplitic nature of (most) of the granite bodies suggests initially high nucleation rates coupled with rapid cooling (Webber et al., 1999). The micro-shear veinlets are considered to have resulted from high pressures in a late volatile- and H_2O-rich phase (post-granite crystallization). There is no mineralogical evidence for H_2O undersaturation in the initial liquid. Even if this was the case, saturation could have occurred in the final stages. Thus with a melt having an H_2O content of 3 wt.%, vapour saturation could occur after some 75% of the body crystallized (Webber et al., 1999). In melts crystallizing at a high level in the crust, such as the Roded quartz diorite, volatile saturation may occur early due to low prevailing load pressure (Candela, 1997). Variations in certain trace elements (e.g., Rb, Sr) among the granite samples may relate to differences in the levels of vapour pressure during crystallization in the separated granite bodies.

The granite retains certain of the I-type characteristics of the quartz diorite, including the ASI values, depletion in Nb, Ti, the enrichment in K, and plot in the VAG field (Rb vs Y + Nb, Fig. 4). Most other oxides and trace elements are either higher in the quartz diorite or the values overlap, with the exception of Sr which is very depleted in the granite.

MMEs are considered by many authors to result from commingling of felsic and mantle mafic liquids (e.g., Barbarin, 1991; Didier and Barbarin, 1991; Seaman and Ramsey, 1992; Vernon, 1991). A similar origin suggests that these enclaves represent hybrid liquids formed by mixing mantle magma with lower crustal melts (e.g., Bussy, 1991; El-Mettwaly, 1993). Aside from the clearly defined metamorphic xenoliths derived either from the country-rock or deeper seated sources, many of the mafic enclaves with igneous textures are MMEs with geochemical characteristics of calc-alkaline, I-type magmas.

7. Conclusions

The quartz diorite formed by fractional crystallization of magma probably derived from melting of a

subduction zone slab. There is little evidence of either magma mixing or large-scale contamination from crustal material. The MMEs show geochemical characteristics of calc-alkaline, I-type magmas. The exposed quartz diorites represent the upper part of a larger pluton in the subsurface, intruded in the waning compressional stages of the northern part of the Neoproterozoic ANS.

The granites formed from late residual liquids in widespread but voluminously small pockets and crystallized toward the end and after the crystallization of the quartz diorite. The granite is rich in elements that show a strong positive correlation with SiO_2 in the quartz diorite (K and Rb) and poor in those with negative correlations (Sr, transition metals, Ca, Mg).

Acknowledgements

We thank Rami Madmon, Ya'acov Raphael and Sa'adya Levy for assistance in the field, Dina Stieber, Olga Joffe and Sarah Ehrlich for the chemical analyses, Micahel Dvorachek for the SEM analyses, and Moshe Peri for the preparations of the thin sections. We are particularly grateful to B. Bonin and A. El-Metwally for the constructive comments.

References

Abdel-Rahman, A.M., 1994. Nature of biotites from alkaline, calc-alkaline, and peraluminous magmas. Journal of Petrology 35, 525–541.

Barbarin, B., 1991. Enclaves of the Mesozoic calc-alkaline granitoids of the Sierra Nevada Batholith, California. In: Didier, J., Barbarin, B. (Eds.), Enclaves and Granite Petrology. Developments in Petrology, 13. Elsevier, Amsterdam, pp. 135–153.

Barker, F., Arth, J.G., 1976. Generation of trondhjemitic-tonalitic liquids and Archaean bimodal trondhjemite-basalt suites. Geology 4, 596–600.

Bentor, Y.K., 1985. The crustal evolution of the Arabo-Nubian Massif with special reference to the Sinai Peninsula. Precambrian Research 28, 1–74.

Bonin, B., Giret, A., 1990. Plutonic alkaline series: Daly gap and intermediate compositions for liquids filling up crustal magma chambers. Schweizerische Mineralogische und Petrographische Mitteilungen 70, 175–187.

Bussy, F., 1991. Enclaves of the Late Miocene Monte Capanne granite, Elba Island, Italy. In: Didier, J., Barbarin, B. (Eds.), Enclaves and Granite Petrology. Developments in Petrology, 13. Elsevier, Amsterdam, pp. 167–178.

Byron, S.J., Atherton, M.P., Hunter, R.H., 1994. The description of the primary textures of Cordilleran granitic rocks. Contributions to Mineralogy and Petrology 117, 65–75.

Candela, P.A., 1997. A review of shallow, ore-related granites: textures, volatiles, and ore metals. Journal of Petrology 38, 1619–1633.

Chappell, B.W., 1999. Aluminium saturation in I- and S-type granites and the characterization of fractionated haplogranites. Lithos 46, 535–551.

Didier, J., Barbarin, B., 1991. The different types of enclaves in granites—Nomenclature. In: Didier, J., Barbarin, B. (Eds.), Enclaves and Granite Petrology. Developments in Petrology, 13. Elsevier, Amsterdam, pp. 19–23.

Drummond, M.S., Allison, D.T., Wesolowski, D.J., 1994. Igneous petrogenesis and tectonic setting of the Elkahatchee quartz diorite, Alabama Appalachians: implications for Penoscotian magmatism in the Eastern Blue Ridge. American Journal of Science 294, 173–236.

El-Mettwaly, A.A., 1993. Microgranular enclaves in the Pan African I-type granites from the Sinai Massif: petrology, mineralogy and geochemistry. Journal of African Earth Sciences 17, 95–110.

Katz, O., Avigad, D., Matthews, A., Heiman, A., 1998. Precambrian metamorphic evolution of the Arabian-Nubian Shield in the Roded area, southern Israel. Israel Journal of Earth Science 47, 93–110.

Kröner, A., 1993. The Pan African Belt of northeastern and eastern Africa, Madagascar, southern India, Sri Lanka and East Antarctica: terrane amalgamation during formation of the Gondwana supercontinent. In: Thorweihe, U., Schandelmeier, H. (Eds.), Geoscientific Research in Northeast Africa. A.A. Balkema, Roterdam, pp. 3–9.

Parada, M.A., Nyström, J.O., Levi, B., 1999. Multiple sources for the Coastal Batholith of central Chile (31–34 °S): geochemical and Sr–Nd isotopic evidence and tectonic implications. Lithos 46, 505–521.

Pearce, J.A., Harris, N.B.W., Tindle, A.G., 1984. Trace element discrimination diagrams for the tectonic interpretation of granitic rocks. Journal of Petrology 25, 956–983.

Peccerillo, A., Taylor, S.R., 1976. Geochemistry of Eocene calc-alkaline volcanic rocks from the Kastamonu area, northern Turkey. Contributions to Mineralogy and Petrology 58, 63–81.

Rapp, R.P., Shimizu, N., Norman, M.D., Appelgate, G.S., 1999. Reaction between slab-derived melts and peridotite in the mantle wedge: experimental constraints at 3.8 GPa. Chemical Geology 160, 335–356.

Seaman, S.J., Ramsey, P.C., 1992. Effects of magma mingling in the granites of Mount Desert Island, Maine. Journal of Geology 100, 395–409.

Segev, A., Goldshmidt, V., Rybakov, M., 1999. Late Precambrian-Cambrian tectonic setting of the crystalline basement in the northern Arabian-Nubian Shield as derived from gravity and magnetic data: Basin-and-Range characteristics. Israel Journal of Earth Science 48, 159–178.

Shaw, A., Downes, H., Thirwall, M.F., 1993. The quartz-diorites of Limousin: elemental and isotopic evidence for Devono-Carboniferous subduction in the Hercynian belt of the French Massif Central. Chemical Geology 107, 1–18.

Stein, M., Goldstein, S.L., 1996. From plume head to continental lithosphere in the Arabian-Nubian Shield. Nature 382, 773–778.

Stern, R.J., 1993. Tectonic evolution of the Late Proterozoic East African orogen: constraints from crustal evolution in the Arabian-Nubian Shield. In: Thorweihe, U., Schandelmeier, H. (Eds.), Geoscientific Research in Northeast Africa. A.A. Balkema, Rotterdam, pp. 73–74.

Stoesser, D.B., Camp, V.E., 1985. Pan-African microplate accretion of the Arabian Shield. Geological Society of America Bulletin 96, 817–826.

Sun, S.-S., McDonough, W.F., 1989. Chemical and isotopic systematics of oceanic basalts: implications for mantle composition and processes. In: Saunders, A.D., Norry, M.J. (Eds.), Magmatism in the Ocean Basins. Blackwell, Oxford, UK, pp. 313–346.

Vernon, R.H., 1991. Interpretation of microstructures of microgranitoid enclaves. In: Didier, J., Barbarin, B. (Eds.), Enclaves and Granite Petrology. Developments in Petrology, 13. Elsevier, Amsterdam, pp. 277–291.

Webber, K.L., Simmons, W.B., Falster, A.U., Foord, E.E., 1999. Cooling rates and crystallization dynamics of shallow level pegmatite-aplite dikes, San Diego County, California. American Mineralogist 84, 708–717.

Weissbrod, T., 1961. The geology and petrology of the Roded massif. M.Sc. Thesis, Hebrew University, Jerusalem, 64p. (in Hebrew).

Wilson, M., 1989. Igneous Petrogenesis. Unwin and Hyman, London, 466p.

Wood, D.A., Joron, J.L., Treuil, M., Norry, M., Tarney, J., 1979. Elemental and variations in basic lavas from Iceland and the surrounding ocean floor. Contributions to Mineralogy anf Petrology 70, 319–339.